Friction **11**(5): 737–747 (2023)
https://doi.org/10.1007/s40544-022-0653-2
ISSN 2223-7690
CN 10-1237/TH

RESEARCH ARTICLE

Drop impact dynamic and directional transport on dragonfly wing surface

Jing XU[1], Wenjun LIU[1], Weixiao SHANG[2], Jun CHEN[2,*], Jiadi LIAN[3]

[1] *School of Mechanical Engineering, Hangzhou Dianzi University, Hangzhou 310018, China*

[2] *School of Mechanical Engineering, Purdue University, West Lafayette, Indiana 47907, USA*

[3] *College of Mechanical and Electrical Engineering, China Jiliang University, Hangzhou 310018, China*

Received: 02 April 2022 / Revised: 05 May 2022 / Accepted: 17 May 2022

Abstract: The ability of dragonflies to fly in the rain without being wetted by raindrops has motivated researchers to investigate the impact behavior of a drop on the superhydrophobic wings of dragonflies. This superhydrophobic surface is used as a reference for the design of directional surfaces and has attracted extensive attention owing to its wide applicability in microfluidics, self-cleaning, and other fields. In this study, the static contact angle and rebound process of a drop impacting a dragonfly wing surface are investigated experimentally, whereas the wetting pressure, Gibbs free energy, and Stokes number vs. coefficient of restitution are theoretically calculated to examine the dynamic and unidirectional transport behaviors of the drop. Results show that the initial inclination angle of the dragonfly wing is similar to the sliding angles along with the drop sliding. The water drop bounces from the bottom of the dragonfly wing to the distal position, demonstrating directional migration. The drop impacts the dragonfly wing surface, and the drop exhibits compression, recovery, and separation phases; in these three phases, the drop morphology evolves. As the Gibbs free energy and cross-sectional area evolve, the coefficient of restitution decreases as the drop continues to bounce, and the Stokes number increases.

Keywords: dragonfly wing; superhydrophobic; wettability; directional transport; bounce

1 Introduction

Drop impact and transport on solid surfaces are ubiquitous in nature and applications, such as microfluidics, self-cleaning, spray painting, anti-icing, and inkjet printing [1–4]. The impact of drops, which was coined by Worthington (1876) [1], can result in drop deposition, bounce [5], or splash [6], and has garnered significant interest among scholars in recent years. Many scholars have begun to investigate the causes of drop rebound and the resulting changes in the corresponding splash. Based on these studies, considering the way of drop transport process, achieving the directional transport of drop, and the development prospects of drop impact are discussed.

Preliminary studies to enable a better understanding of liquid drop-to-solid collisions have been conducted. The results show that surface superhydrophobicity [7], the Leidenfrost effect [8], substrate sublimation [9], and ambient pressure reduction [10] can facilitate drop rebound, particularly the effect of superhydrophobicity. Liu et al. [11, 12] discovered that at the same micron scale, the conical micron structure significantly enhanced the ability of an impinged drop to rebound in the shape of a circular cake, resulting in a shorter solid–liquid contact time and less energy dissipated by the impinged drop. Van der Veen et al. [13] investigated the height and distance effects of the microstructure of a hydrophobic surface on an air film based on the development of an air film between the collision drop and a wall. Yeong et al. [14] investigated the spreading and rebounding characteristics of a

* Corresponding author: Jun CHEN, E-mail: junchen@purdue.edu

drop-hitting plane and an inclined superhydrophobic surface and discovered that the viscosity and retreat angle can change the rebound characteristics of the drop. Hao et al. [15] systematically investigated the relationship between the critical velocity from the drop impact process and the microgeometric structure of a superhydrophobic surface. Khojasteh et al. [16] introduced potential applications of superhydrophobic surfaces and the most recent progress pertaining to the dynamics and kinematics of drop-impacting superhydrophobic substrates. LeClear et al. [17] discussed the dynamic behavior of a drop on an inclined superhydrophobic surface and concluded that the Weber number is related to the impact dynamics on an inclined surface featuring three different types of textures. Jiang et al. [18] experimentally investigated the effect of a drop on superhydrophobic surfaces with or without protuberances and discovered that the existence of protuberances not only changed the impact dynamics, but also significantly affected drop deformation. However, these studies pertaining to the bouncing behavior of drops impacting hydrophobic surfaces of different materials and structures focused more on the effect of surface structure on drop impact. Few studies have investigated the impact of a drop on the transport surface.

After 3.5 billion years of biological evolution and co-evolution, organisms have optimized their structures, shapes and functions, and movement modes and behaviors, thus providing a scientific basis for the selection of technical schemes and the development of self-compensating, self-adapting, and self-regulating technologies. Consequently, the field of biomimetics was birthed. Rice leaves, lotus leaves, butterflies, and dragonflies exhibit excellent hydrophobic properties. Pan et al. [19] and Kulinich and Farzaneh [20] discovered that the lotus leaf surface not only features numerous micron-sized papillae, but is also abundant in waxy materials of low surface energy, thus affording superhydrophobicity on the lotus leaf. Pu et al. [21] discovered that rice features a micro–nano composite structure similar to that of the lotus leaf surface. Sun et al. [22] discovered that the micron-sized papillae on a lotus leaf surface were distributed evenly, whereas the papillae on a rice leaf surface were distributed orderly parallel to the leaf edge. Zhang et al. [23] and Ye et al. [24] showed that the micropores on a butterfly wing surface and the nano-sized columnar structure on the cicada wing surface contributed significantly to the superhydrophobic properties of those surfaces. Ren and Li [25] introduced the functional characteristics of a dragonfly wing, described the effects of its shape, construct, structure, and material on the functional characteristics, and proposed its application prospects. Gao et al. [26] designed a bionic surface structure based on a dragonfly wing to enhance the suspension lift of a glass-transport unit. Dragonflies are not wetted by rain during flight, which involves raindrop impact and transport. Hence, researchers are motivated to investigate the impact behavior of drops on their superhydrophobic airfoil surfaces, which significantly affects the directional surface design. However, the microstructure of a dragonfly's wing surface and its effect on drop impact and transport performance are yet to be elucidated. Most studies focused on the behavior of fluid motion on the biological surface but did not investigate the motion mechanism. Studies regarding the unique structure of the dragonfly wing surface and its correlation with liquid motion have been even less published, thus greatly affects the extraction and application of the superhydrophobic wing surface of dragonfly wings.

In this study, the dragonfly wing surface is considered as the research object, the static contact angle and rebound process of drop impact are investigated experimentally, and the wetting pressure, Gibbs free energy, and Stokes number vs. coefficient of restitution are theoretically calculated to examine the dynamic and unidirectional transport behaviors of drops impacting the dragonfly wing surface. The relationship among the solid drop impact, transport characteristics, and wettability is discussed, and the properties of controllable fluid transport on dragonfly wings are revealed, thus providing a theoretical basis and rationale for the formation of unpowered self-driven microflow channel systems.

2 Experimental

2.1 Sample preparation

Test samples of wing membranes were obtained from dragonflies. A Philips XL30 scanning electron

microscopy(SEM; S-4800, Hitachi) equipment was employed to investigate the morphology and microstructure of the dragonfly wings, all of which were coated with 8 nm of gold. Finally, the samples were observed via SEM (Fig. 1(c)). As shown in Fig. 1(c), dragonfly wings feature multilevel micro and nano structures attached to hydrophobic wax cuticles growing on their surface, which is a unique low-dimensional biological structure that endows them with excellent superhydrophobic properties. Additionally, it allows the droplets to tower over the surface of the dragonfly wings (Figs. 1(a) and 1(b)). Thus, when a droplet hits a dragonfly wing, it undergoes the stages of compression, recovery, separation, and rebounding (Fig. 1(d)).

2.2 Experimental apparatus

A series of uniform drops of distilled water was deposited onto the sample. A pressure tank filled with water was used to supply fluid via the pipe to the nozzle, which featured an inner diameter of 0.15 mm. A high-speed camera (Phanto V7, Vison Research, Inc.) with a recording rate of 5,000 frames/s, equipped with a Nikon 60 mm lens, was used to capture the post-impingement process using a back-illumination technique, as shown in Fig. 2. The surface tension, viscosity, and density of the liquid drops were 7.275 × 10^{-2} N/m, 1.005 × 10^{-3} Pa/s, and 9.98 × 10^{3} kg/m, respectively. The impact velocity of the drop

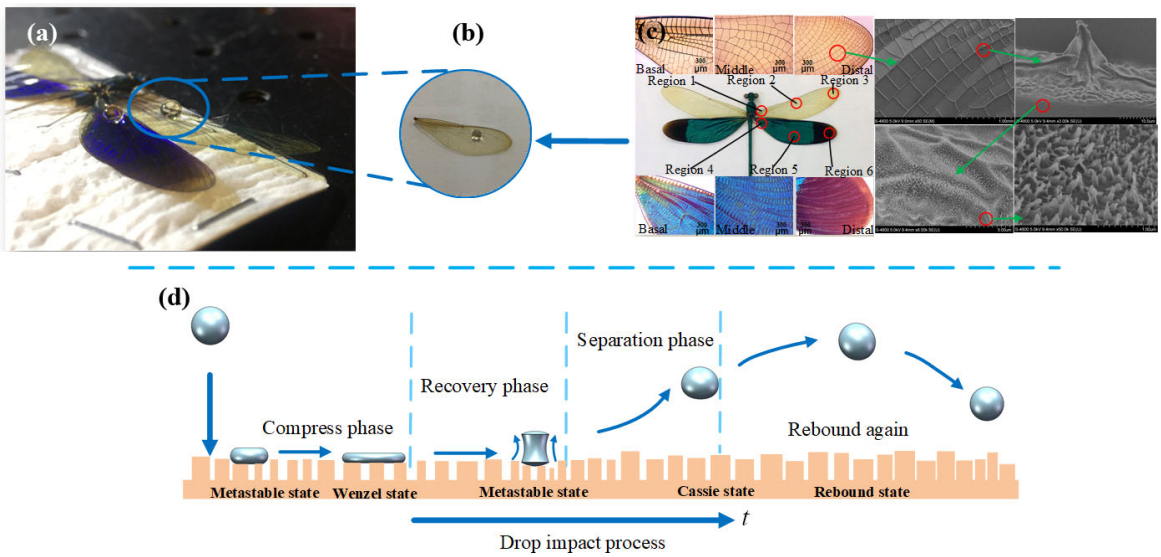

Fig. 1 Microstructure of dragonfly wings and diagram showing droplet impact motion on dragonfly wings. (a) Droplets collapsed onto surface of dragonfly wings. (b) Details of liquid bead on surface of dragonfly wing. (c) Structure and micromorphology of various section of dragonfly wing. (d) Model depicting motion of droplet on surface of dragonfly wing during each stage of impact, and the corresponding state of motion at each stage.

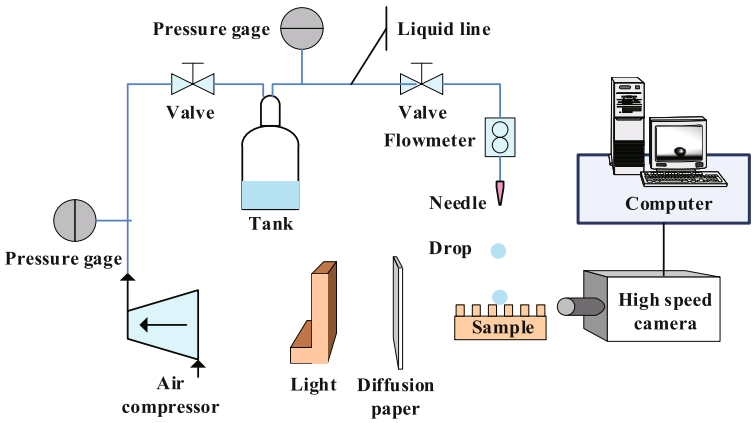

Fig. 2 Schematic illustration of water drop-impacting experimental apparatus.

was controlled by changing the distance between the needle and sample in the vertical direction (distance of 20 mm).

3 Results and discussion

3.1 Static contact angle

The drop did not stop moving and rolled off easily along the radial outward (RO) direction of the surface owing to the small tilt of the real wing surface. Therefore, the dragonfly wing was tilted on a glass slide to investigate the effect of the dragonfly wing structure on the wettability. Figure 3 shows the static contact angles of a 3 μL drop at different positions on the dragonfly wing surface. The dragonfly wing structure exhibited superhydrophobicity with static contact angles exceeding 150° at three positions on the surface in a transient state. The advancing contact angle (from 153° to 150°) decreased along the RO direction (from the basal position to the distal position), and the sliding angles were 3°–4°. Hence, there are reasons to believe that the initial angle of inclination of the dragonfly wing was similar to the sliding angle along the RO direction. Considering the motion of the dragonfly, when the wing was tilted down along the RO direction, the liquid drop overflowed the ridge of the dragonfly wing and departed rapidly from the wing. By contrast, when the wing was tilted up against the RO direction, the liquid pinned at the ridge edge with a larger contact angle until the next swing.

3.2 Drop impact process

3.2.1 *Theoretical model*

When a liquid drop impacts a solid surface, the bouncing behavior of the drop depends on its surface hydrophobicity. For a superhydrophobic surface, the liquid repels the surface, and the drop may continuously rebound several times until it stops on the surface (Fig. 4(a)); furthermore, the bouncing state depends on the wetting pressure. For more details, please see Section S1 of the Electronic Supplementary Material (ESM).

3.2.2 *Maximum rebound height*

The surface of dragonfly wings exhibits superhydrophobic properties; therefore, the droplets will bounce continuously when they strike the surface of the dragonfly wings. Figure 4(b) shows that the maximum rebound height of a drop that rebounded completely on the dragonfly wing surface in the vertical direction. The drop impacted the dragonfly wing surface, occurring in completely rebound. When time t = 71 ms, the drop rebounded to the maximum height, which decreased as t increased. Kinetic energy was dissipated owing to the deformation during the entire drop rebound process.

3.3 Transport process

Figure 4(e) shows the maximum migration distance of a drop impacting the dragonfly wing surface in the horizontal direction. The results show that the drop underwent lateral transport, and that the lateral migration distance decreased as t increased. The water drop bounced from the basal position to the distal position of the dragonfly wing, and the surface presented unidirectional transport characteristics. Considering the nano and micro textures of the dragonfly wing surface (Fig. 1(c)) as well as the static contact angles of different sections of the dragonfly wing surface (Fig. 3), the contact angles decreased along the RO direction (from the basal to the distal region of the dragonfly wing), and an interfacial energy gradient appeared on the dragonfly wing surface. The different contact angles of the water drop resulted in unbalanced tension in the gas–liquid–solid three-phase contact line, and the driving force (F are provided

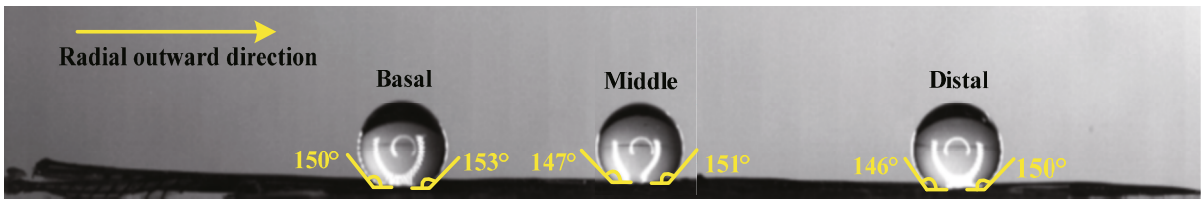

Fig. 3 Static contact angles of 3 μL drop at different positions on dragonfly wing surface.

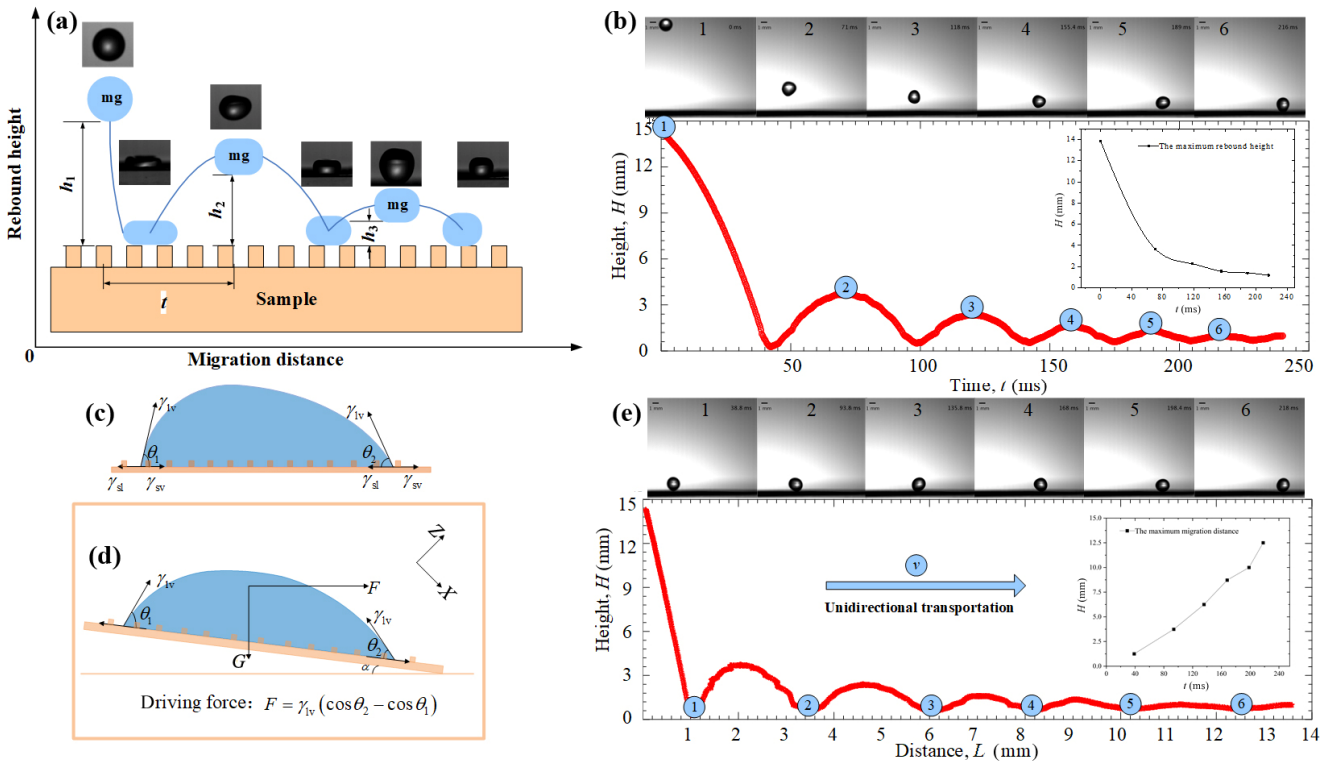

Fig. 4 Theoretical model and experimental data diagram showing bounce and transport of liquid droplets on surface of dragonfly wing bladder in presence of force. (a) Tentative description of rebound height and migration throughout impact process, and "mg" represents the gravity of the drop. (b) Complete rebound phenomenon of drop on dragonfly wing surface in vertical direction (maximum rebound height). Analysis of drop forces in different planes: (c) Analysis of plane drop force; (d) *X*-axis gravity analysis on inclined surface; (e) transport of drop impacting dragonfly wing surface in horizontal direction (maximum migration distance).

in Section S2 of the ESM) along the direction of interfacial energy increased, thus resulting in drop migration (Fig. 4(c)). Therefore, drop migration occurred on a solid surface along the direction of decreasing contact angles when the driving force of the drop exceeded the resistance force of the drop.

In addition, a tilt angle was observed in the initial dragonfly wing surface, and the gravitational force F_{mg} along the *X*-axis should be considered in the force analysis (Fig. 4(d)) as it significantly affects lateral drop transport. When the drop tilted on the dragonfly wing surface, it was expelled from the dragonfly wing surface owing to gravity. Therefore, the drop can be designed to be horizontally transported, similar to a real wing surface.

3.4 Drop continuous bounce evolution

Figures 5(a) and 5(b) show rebound images of a drop on the dragonfly wing surface at the first rebound and a process diagram showing a drop before and after impacting the dragonfly wing surface, respectively. The results show the wetting state transition among the Cassie, Wenzel, and metastable states, and three phases throughout the impact process: the compression phase (Cassie–Metastable–Wenzel state, 39 ms < *t* < 43 ms), recovery phase (Wenzel–Metastable–Cassie state, 43 ms < *t* < 48 ms), and separation phase (Cassie-rebound state, 48 ms < *t* < 74 ms). After the drop impacted the surface, the micro and nano surfaces limited the bounce of the drop. In the compression phase, where the drop was compressed during impact, some of liquid from the drop extruded into the microstructure, the impacting drop collided with the surface and formed an expanding sheet, the drop reached the maximum spreading radius at 43 ms, and the spread velocity decreased as time progressed until it reached zero. During the compression phase, the contact pressure increased and evolved depending on the wetting state. A wetting pressure

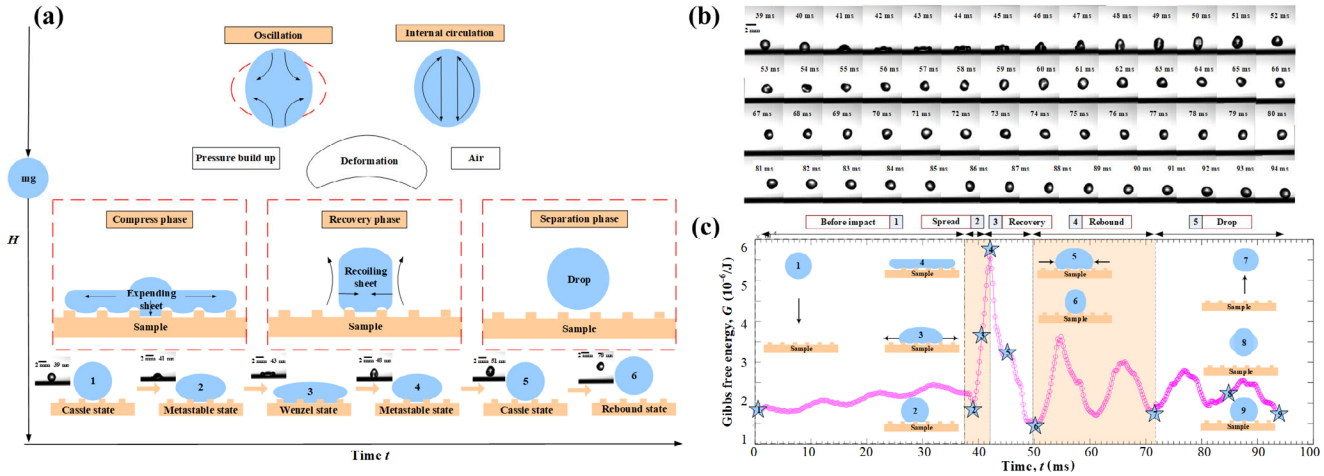

Fig. 5 Theoretical model and experimental impact images of droplet morphology change during droplet impact and experimental data showing change in Gibbs free energy of droplet with time. (a) Process diagram showing drop before and after impacting dragonfly wing surface. (b) Impact phase image of drop on dragonfly wing surface during the first rebound. (c) Drop shape evolution vs. time of drop impacting dragonfly wing surface from Stage 1 (before impact) to Stage 5 (drop) during Rebound 1.

was observed between the drop and contact surface (the wetting pressure included the dynamic pressure P_D = 0.15 kPa and instantaneous water hammer pressure P_H = 0.16 MPa), as well as an anti-wetting pressure (anti-wetting pressure P_C of 0.22 MPa–0.6 kPa). This anti-wetting pressure occurred in the non-wetting state ($P_C > P_H > P_D$), where the Cassie–Metastable–Wenzel state transition occurred, and the Gibbs free energy G from $G_{star\text{-}2}$ to $G_{star\text{-}4}$ increased ($G_{star\text{-}2}$ is the star numbered 2 spread in Fig. 5(c)). At 43 ms < t < 48 ms, the drop entered the recovery phase because of the surface tension, capillary force, and some simultaneous internal circulations inside the drop. The drop formed a recoiling sheet, the Wenzel–Metastable–Cassie state transition occurred, and the Gibbs free energy G from $G_{star\text{-}4}$ to $G_{star\text{-}6}$ decreased (Fig. 5(c)). When t > 48 ms, the drop began to rebound, and the bouncing state depended on the wetting pressure. This is named the separation phase, where the kinetic energy of the drop is converted into potential energy. The bounce of the drop broke the three-phase interface, the transition of the Cassie-rebound state occurred, and the drop bounced at a maximum height at 74 ms. This is because the drop struck the superhydrophobic wall surface, which allowed the drop and wall to suction more gas, the gas was compressed in the microstructure, the formed high-pressure gas layer hindered the downward movement of the drop, the spreading speed was low, and the energy loss due to the interaction with the wall was insignificant, thus resulting in sufficient energy for the drop to rebound. After the drop rebounded to the maximum height, it descended under the action of gravity and struck the dragonfly wing surface again in the next rebound process.

The drop underwent six rebound phases, where different shapes and cross-sectional area of the drop were exhibited at each stage. Figures 6(a) and 6(b) show the Gibbs free energy G and section area S of a drop as a function of t, respectively, where 12 points are used to present the maximum and minimum section areas in the six rebound processes. The results show that the minimum transient area under the compression stage increased gradually as the number of impacts increased, whereas the Gibbs free energy decreased gradually. The maximum contact area of the drop in the recovery phase decreased after a complete rebound, and the Gibbs free energy increased gradually, although the overall change was insignificant. For Rebound 1 (t = 40–50 ms), the drop spread at Point 1, the minimum S was 2.2 mm^2, and the initial S was 4.4 mm^2. The drop morphology evolved because of the surface tension and capillary forces, thus causing the potential and kinetic energies of the drop to be converted; at this time, the maximum G was 5.9 × 10^{-6} J when the drop rebounded, and the drop failed to rebound immediately because of the adsorption force. Additionally, it was stretched to

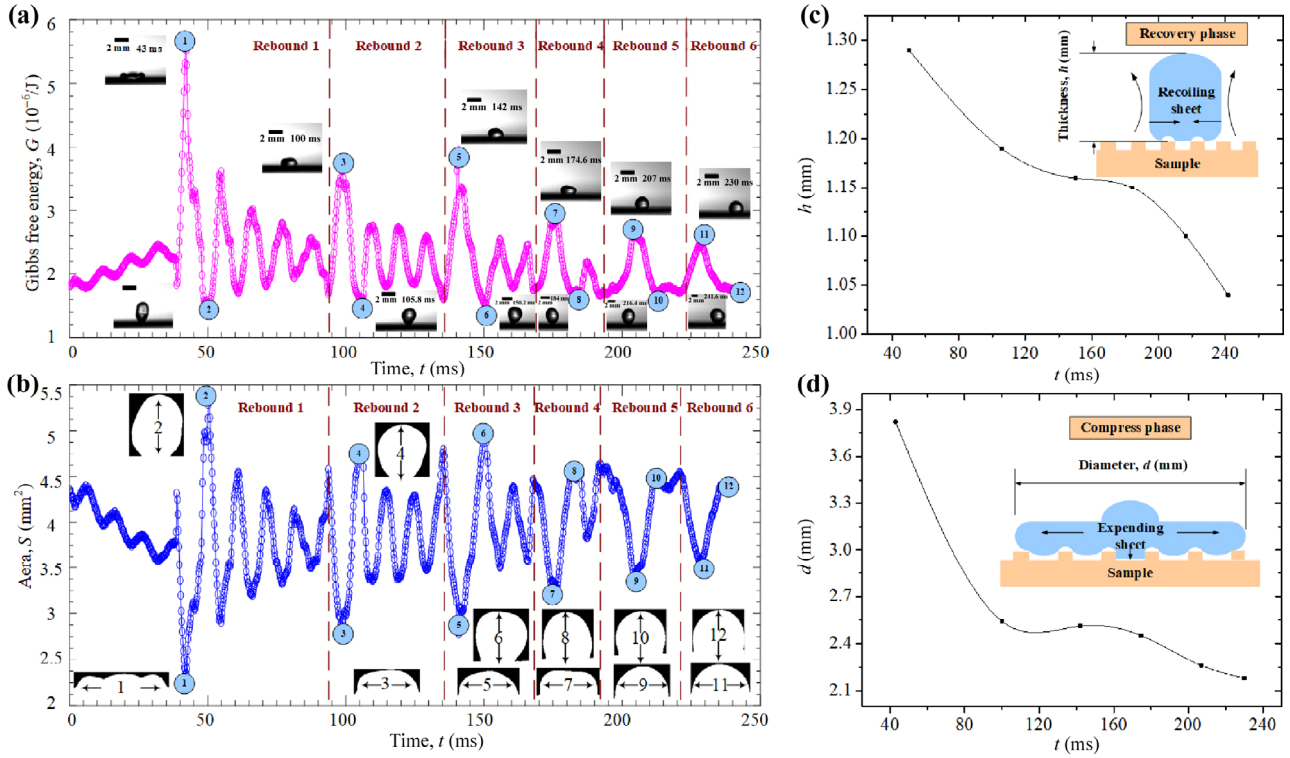

Fig. 6 Experimental data plots of Gibbs free energy, maximum cross-sectional area of droplets, maximum spreading diameter, and maximum recoiling thickness of droplets in six rebound phases. (a) Gibbs free energy G vs. t of droplet impacting dragonfly wing surface. (b) S vs. t of drop impacting dragonfly wing surface. Maximum spreading diameter d and maximum recoiling thickness h vs. t of drop impacting dragonfly wing surface. (c) Variation curve of the maximum recoiling thickness h in recovery phase in six rebound phases. (d) Variation curve of the maximum spreading diameter d in compression phase in six rebound phases, and "D" represents the drop diameter.

form a weak liquid column, its S reached a maximum value at Point 2, i.e., 5.5 mm^2, whereas its G was minimum, i.e., 1.2×10^{-6} J.

At t = 95 ms, the drop entered Rebound 2. Its G decreased, and its compression degree decreased because of the energy consumed in Rebound 1. $S_{\text{point-3}}$ was 2.75 mm^2, which was larger than $S_{\text{point-1}}$, whereas $G_{\text{point-3}}$, which was 3.8×10^{-6} J, was lower than $G_{\text{point-1}}$. $S_{\text{point-4}}$, which was 4.75 mm^2, was smaller than $S_{\text{point-2}}$, whereas $G_{\text{point-4}}$, which was 1.4×10^{-6} J, was slightly greater than $G_{\text{point-2}}$. As the drop rebounded, the difference between S and G in the spreading and rebounding phases decreased gradually. This is attributed primarily to the stable morphological change of the drop, as well as the decrease in the kinetic potential energy change. In Rebound 6, the difference between the maximum and minimum S of the drop reduced to 1 mm^2, and the difference between the maximum and minimum G of the drop reduced to 1.4×10^{-6} J.

Figures 6(c) and 6(d) show that the maximum recoiling thickness h and maximum spreading diameter d of the drop during the compression and recovery phases decreased gradually with time, and that the trends are distributed within a wide range. Figure 6(c) shows that at t = 45 ms, the recoiling thickness of the drop was maximum (h = 1.8 mm) during the recovery stage, and the drop shape returned gradually to an oval shape under the actions of surface tension and capillary force. The elliptical shape suppressed the bouncing amplitude, the energy of the drop was consumed, h_{maximum} decreased, and the trend became smoother. During the recovery stage at approximately 240 ms, h_{maximum} was 1.04 mm. Figure 6(d) shows that the drop exhibited an elliptical shape when it spread to the maximum d (d = 3.86 mm) in the compression stage. After the drop reached the compression stage of Rebound 2, the maximum d decreased rapidly to 2.5 mm at 100 ms owing to the energy consumed in Rebound 1. As drop energy E decreased, the

decreasing trend decelerated after the droplet bounced continuously until it reached the minimum d = 2.15 mm at 230 ms. When the total energy exceeded the initial surface and gravity at the maximum d, the drop rebounded from the surface.

3.5 Elastohydrodynamic rebound

Details regarding the relevant Stokes number St and coefficient of restitution β are provided in Section S3 of the ESM.

Figure 7 shows the β vs. St of a water drop impacting the dragonfly wing surface for six rebound times. The results show that the actual experimental curve presents six continuous circles, which correspond to six complete rebound times of the drop. The drop was regarded as a particle, and the fluid was a gas. According to definition, St changed depending on the drop shape. For the six rebounding drops, the higher rebound height of a previous drop compared with the rebound height of the subsequent drop yielded a larger St. In particular, h was larger in the first rebound stage, and the drop reached the maximum velocity when approaching the wall. The impact was significantly affected by inertia, the height of the rebound drop was close to h, and the effect of wall viscosity on the impact was insignificant. Therefore, St and β changed the most during Rebound 1 (St = 35–132; β = 0.947–1.036). The range of β decreased as the drop continued rebounding because the rebound height of the previous drop was greater, and the rebound height determines the instantaneous impact velocity and St. The previous rebound drop suctioned more liquid and air into the surface texture during the impact process with a large impact force, thus causing the liquid drop to be deformed significantly, as well as greater energy loss and a lower β at higher St. At the final rebound (Rebound 6), the curve was a small flat circle with a St of approximately 31, and β was within a small range (β = 0.995–1.004), with a final value of approximately 1. These results are consistent with the experimental results.

4 Conclusions

1) The dragonfly wing surface exhibited superhydrophobicity with static contact angles exceeding 150°. The advancing contact angle of the drop decreased along the RO direction, and the sliding angles were 3°–4°. The drop exhibited directional migration characteristics, and the lateral migration distance of the drop decreased as t increased.

2) The impact process comprised phases (compression, recovery, and separation). During the compression phase, the contact pressure increased and changed depending on the wetting state, it is the non-wetting state ($P_C > P_H > P_D$). The minimum transient area increased gradually with the number of impacts, and the Gibbs free energy decreased gradually. Subsequently, the drop entered the recovery phase because of the surface tension and capillary force, which formed a recoiling sheet, the maximum contact area decreased, and the Gibbs free energy increased gradually. In the separation phase, the kinetic energy of the drop converted into potential energy, and the area increased.

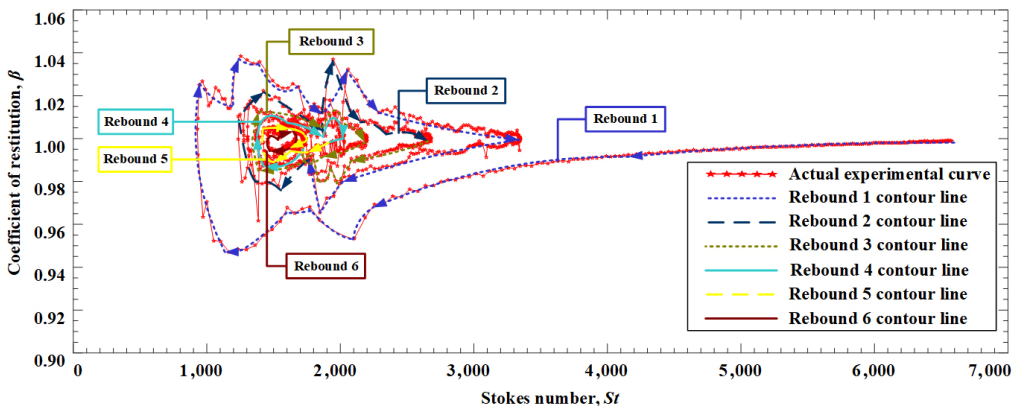

Fig. 7 Coefficient of restitution β vs. Stokes number St of water drop impacting dragonfly wing surface.

3) The drop impacted the dragonfly wing surface and rebounded six times, and the experimental curve showed six consecutive circles. Meanwhile, St and β changed the most during Rebound 1 (St = 35–132; β = 0.947–1.036). The measured range of rebound β decreased as the drop continued to bounce. Because of the energy consumed during the drop impact, St was approximately 31, and β was within a small range (β = 0.995–1.004), with a final value of approximately 1. These results were consistent with the experimental results.

Acknowledgements

The research is financially supported by the Fundamental Research Funds for the National Natural Science Foundation of China (No. 52275182) and Provincial Universities of Zhejiang, China (No. GK229909299001-14).

Electronic Supplementary Material: Supplementary material is available in the online version of this article at https://doi.org/10.1007/s40544-022-0653-2.

References

[1] Moreira A L N, Moita A S, Panão M R. Advances and challenges in explaining fuel spray impingement: How much of single droplet impact research is useful? *Prog Energy Combust Sci* **36**(5): 554–580 (2010)

[2] Derby B. Inkjet printing of functional and structural materials: Fluid property requirements, feature stability, and resolution. *Annu Rev Mater Res* **40**: 395–414 (2010)

[3] Rukosuyev M V, Barannyk O, Oshkai P, Jun M B G. Design and application of nanoparticle coating system with decoupled spray generation and deposition control. *J Coat Technol Res* **13**(5): 769–779 (2016)

[4] Zhou Z F, Chen B, Wang R, Wang G X. Comparative investigation on the spray characteristics and heat transfer dynamics of pulsed spray cooling with volatile cryogens. *Exp Therm Fluid Sci* **82**: 189–197 (2017)

[5] Yun S, Choi W, Choi D S. Bouncing characteristics of an elliptical footprint drop on a solid surface. *Int J Heat Mass Transf* **126**: 854–860 (2018)

[6] Yang H, Sun K, Xue Y, Xu C W, Fan D Y, Cao Y, Xue W. Controllable drop splashing on picosecond laser patterned hybrid superhydrophobic/-philic surfaces. *Appl Surf Sci* **481**: 184–191 (2019)

[7] Mitra S, Evans G. Dynamic surface wetting and heat transfer in a droplet-particle system of less than unity size ratio. *Front Chem* **6**: 259 (2018)

[8] Jowkar S, Morad M R. Rebounding suppression of droplet impact on hot surfaces: Effect of surface temperature and concaveness. *Soft Matter* **15**(5): 1017–1026 (2019)

[9] Antonini C, Bernagozzi I, Jung S, Poulikakos D, Marengo M. Water drops dancing on ice: How sublimation leads to drop rebound. *Phys Rev Lett* **111**(1): 014501 (2013)

[10] Wang J, Yang P, Lubrecht A A, Kaneta M. Numerical investigation of thermal EHL in elliptical contact under impact motion. *Proc Inst Mech Eng Part J J Eng Tribol* **229**(9): 1125–1131 (2015)

[11] Liu Y H, Whyman G, Bormashenko E, Hao C L, Wang Z K. Controlling drop bouncing using surfaces with gradient features. *Appl Phys Lett* **107**(5): 051604 (2015)

[12] Liu Y H, Moevius L, Xu X, Qian T, Yeomans J M, Wang Z. Pancake bouncing on superhydrophobic surfaces. *Nat Phys* **10**(7): 515–519 (2014)

[13] Van der Veen R C A, Hendrix M H W, Tran T, Sun C, Tsai P A, Lohse D. How microstructures affect air film dynamics prior to drop impact. *Soft Matter* **10**(21): 3703–3707 (2014)

[14] Yeong Y H, Burton J, Loth E, Bayer I S. Drop impact and rebound dynamics on an inclined superhydrophobic surface. *Langmuir* **30**(40): 12027–12038 (2014)

[15] Hao P F, Lv C J, Niu F L, Yu Y. Water droplet impact on superhydrophobic surfaces with microstructures and hierarchical roughness. *Sci China Phys Mech Astron* **57**(7): 1376–1381 (2014)

[16] Khojasteh D, Kazerooni M, Salarian S, Kamali R. Droplet impact on superhydrophobic surfaces: A review of recent developments. *J Ind Eng Chem* **42**: 1–14 (2016)

[17] LeClear S, LeClear J, Abhijeet, Park K C, Choi W. Drop impact on inclined superhydrophobic surfaces. *J Colloid Interface Sci* **461**: 114–121 (2016)
[18] Jiang X F, Xu E L, Wu G G, Li H Z. Drop impact on superhydrophobic surface with protrusions. *Chem Eng Sci* **212**: 115351 (2020)
[19] Pan H B, Wang C D, Yu H B, Liu J X. Progress in preparation and application of superhydrophobic surface. *New Chem Mater* **42**(7): 208–210 (2014) (in Chinese)
[20] Kulinich S A, Farzaneh M. Ice adhesion on super-hydrophobic surfaces. *Appl Surf Sci* **255**(18): 8153–8157 (2009)
[21] Pu X, Ge J F, Chen C C. Brief introduction to the research on biomimetic super-hydrophobic surface. *Guangdong Chem Ind* **37**(5): 25–28, 40 (2010) (in Chinese)
[22] Sun T L, Feng L, Gao X F, Jiang L. Bioinspired surfaces with special wettability. *Acc Chem Res* **38**(8): 644–652 (2005)
[23] Zhang H M, Wang T, Yu Y H, Zhang D B, Pan J F. Preparation and hydrophobic properties of the micro-nano structure of butterfly wing surface. *China Surf Eng* **27**(5): 131–136 (2014) (in Chinese)
[24] Ye X, Zhou M, Li J, Liu H X, Yuan R, Yang H F, Li B J, Cai L. Microstructure of superhydrophobic surfaces from natural to artificial. *Nanotechnol Precis Eng* **7**(5): 381–386 (2009) (in Chinese)
[25] Ren L Q, Li X J. Functional characteristics of dragonfly wings and its bionic investigation progress. *Sci China Technol Sci* **56**(4): 884–897 (2013)
[26] Gao S Y, Zhang B C, Sun J W, Liu W R. A disigned method of the surface structure of suspended glass transport device based bionic structure of dragonfly wings. *Ind Lubr Tribol* **72**(10): 1245–1250 (2020)

Jing XU. She received her Ph.D. in chemical process mechanics from Zhejiang University of Technology, China, in 2014. She joined Hangzhou Dianzi University, China, in 2014 and now is an associate professor at the School of Mechanical Engineering, Hangzhou Dianzi University, China. She was a visiting scholar at Purdue University, USA (2018.09–2019.09). Her research areas include intelligent fluid transport, surface technology, friction, and lubrication.

Wenjun LIU. He received his B.E. degree in engineering from Jiangxi University of Technology (Nanchang), China, in 2019. He is now a graduate student of mechanical engineering in Hangzhou dianzi University, China. His research mainly focuses on surface microstructure.

Weixiao SHANG. He is currently a Ph.D. candidate at the School of Mechanical Engineering, Purdue University, USA. He received his master degree at the School of Aeronautics and Astronautics, Purdue University, in 2014. His research interests include advanced flow diagnostics techniques, impinging sheet, and atomization.

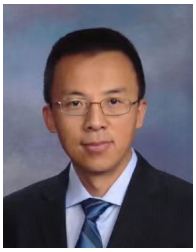

Jun CHEN. He is a professor of mechanical engineering at Purdue Unviersity, USA. He received his Ph.D. degree in mechanical engineering from Johns Hopkins University, USA, in 2005. His research areas cover flow diagnostic techniques, unsteady flow measurements and analysis, turbulence modeling, low Mach number aeroacoustics, stratified flows, and cardiovascular flow and hemodynamics.

Jiadi LIAN. He received his Ph.D. degree from Zhejiang Sci-Tech University, China, and now is a teacher in the School of Mechanical and Electrical Engineering of China Jiliang University. His research fields include intelligent fluid transmission, surface technology, friction, and lubrication.